

Hugoniot equation of state and sound velocity of CaSiO₃ glass under shock compression

Ye Wu ¹, Qing Zhang ¹, Yishi Wang ¹, Yu Hu ¹, Zehui Li ¹, Zining Li ¹, Chang Gao ¹, Xun Liu ¹, Haijun Huang ¹, Yingwei Fei ²

¹ School of Physics and Mechanics, Wuhan University of Technology, Wuhan, Hubei 430070, China

² Earth and Planets Laboratory, Carnegie Institution for Science, Washington, DC 20015, USA

Corresponding author: Xun Liu (xun_liu@whut.edu.cn) and Yingwei Fei (yfei@carnegiescience.edu)

Abstract

Davemaoite, as the third most abundant mineral in the lower mantle, constitutes significant amounts in pyrolite and mid-ocean ridge basalts. Due to its unquenchable nature, measurements by static compression techniques on physical properties of davemaoite at lower mantle conditions are rare and technically challenging, and those are essential to constrain compositions and properties of mineralogical models in the lower mantle. Here, we present Hugoniot equation of state and sound velocity of CaSiO_3 glass under shock compression. The CaSiO_3 glass transforms into the crystalline phase above 34 GPa and completely transforms into davemaoite above 120 GPa. Thermal equation of state and Hugoniot temperature of davemaoite have been derived from the shock wave data. The CaSiO_3 glass under shock compression has very high shock temperature. Shock wave experiments for sound velocity of CaSiO_3 glass indicate that no melting is observed at Hugoniot pressure up to 117.6 GPa. We propose that the melting temperature of davemaoite should be higher than those reported theoretically by now.

1 Introduction

Knowledge of the mineralogy of the Earth's interior is crucial to understand the structure, composition and dynamical evolution of the Earth [Hofmann, 1988; Kaminski and Javoy, 2013; Lee *et al.*, 2010]. Due to limited deep samples available in nature, experiments and theoretical calculations on structures, properties and behaviors of minerals are dominate strategies to constrain the compositions and properties of mineralogical models in the lower mantle [Fei and Tracy, 2024; Price, 2010; Wentzcovitch and Stixrude, 2018]. High pressure experiments on density and sound velocity of mantle minerals provide significant information on mineralogy of the deep mantle by comparisons with the observed seismic velocities [Fukao and Obayashi, 2013; Garnero *et al.*,

2016; Waszek *et al.*, 2018]. Laboratory measurements on structures and properties of the deep minerals have benefited from the rapidly evolving of high pressure science and technology [Mao *et al.*, 2016; Shen and Wang, 2014; Shen and Mao, 2016]. The major lower mantle minerals, bridgmanite and ferropericlase, have received very extensive experimental and theoretical investigation due to its importance and significance in the lower mantle [Murakami *et al.*, 2024; Tschauner *et al.*, 2014]. However, a major uncertainty in mineralogical models of the lower mantle is davemaoite, the third most abundant mineral in the lower mantle [Tschauner *et al.*, 2021].

Davemaoite, also known as CaSiO_3 perovskite, comprises up to 10 vol.% of pyrolite and 30 vol.% of mid-ocean ridge basalts in the Earth's lower mantle [Irifune, 1994; Irifune *et al.*, 2010; Ricolleau *et al.*, 2010]. Its existence has been demonstrated by means of analysis of superdeep diamond inclusions [Tschauner *et al.*, 2021]. Davemaoite with a cubic structure (space group: $Pm\bar{3}m$) is stable along a typical mantle geothermo [Liu and Ringwood, 1975]. But davemaoite is unquenchable and it transforms into the tetragonal phase (space group: $I4/mcm$) upon quenching temperature below about 500 K at high pressures [Komabayashi *et al.*, 2007; Sagatova *et al.*, 2021; Shim *et al.*, 2000; Wu *et al.*, 2024]. The unquenchable nature of davemaoite at ambient conditions makes reliable measurements of its physical properties to be technically challenging, thus most studies of davemaoite focus on thermal equation of state through static compression techniques and theoretical calculations. The thermoelastic parameters of davemaoite have been reported by a series of static experiments and theoretical calculations [Kawai and Tsuchiya, 2014; Noguchi *et al.*, 2013; Shim *et al.*, 2000; Sun *et al.*, 2016; Wang *et al.*, 1996; Zhang *et al.*, 2006], although discrepancy among them exists and has been discussed [Sun *et al.*, 2016]. Since davemaoite is unstable at ambient conditions, there are few experimental studies on its sound velocity at lower mantle pressure and temperature (P-T) conditions despite its importance in the lower mantle. In

2019, two studies successively reported sound velocities of davemaoite measured by means of ultrasonic-interferometry coupled with multi-anvil press [Gráaux *et al.*, 2019; Thomson *et al.*, 2019]. But the P-T conditions are only 23 GPa and 1700 K, corresponding to the uppermost lower mantle. Several theoretical studies on elasticity and sound velocities of davemaoite have been proposed but also encountered controversy due to different calculation methods [Karki and Crain, 1998; Kawai and Tsuchiya, 2015; Li *et al.*, 2006; Stixrude *et al.*, 2007]. Davemaoite is considered to be related to the large low-shear-velocity provinces in the lower mantle and mid-mantle discontinuities [Immoor *et al.*, 2022; Thomson *et al.*, 2019]. The previous experimental P-T conditions on sound velocity measurements are lower than those in the deep lower mantle, and sound velocities of davemaoite in the lower mantle are obtained by extrapolation based on limited experimental data and thermodynamic model. The extrapolated sound velocities from the only two studies show great difference and are all lower than those from theoretical calculations [Thomson *et al.*, 2019].

In view of the unquenchable nature and significance of davemaoite, here, we propose the study of Hugoniot equation of state and sound velocity of CaSiO_3 glass under shock compression. The CaSiO_3 glass is used as the initial material of shock wave experiments. High pressure and high temperature conditions under shock compression promote the transformation of CaSiO_3 glass to davemaoite. Shock wave experiments for Hugoniot and sound velocity have been performed up to 79.2 GPa and 117.6 GPa, respectively. The thermodynamic parameters and Hugoniot temperature of davemaoite have been derived according to shock wave data. Sound velocities of davemaoite along Hugoniot have also been discussed.

2 Experimental Methods

2.1 Sample preparation and characterization

Starting materials of CaSiO_3 glass were prepared using reagent grade CaCO_3 (Alfa Aesar, 99.5%) and SiO_2 (Alfa Aesar, 99.8 %) with the molar ratio of 1 : 1. The starting materials were thoroughly mixed and decarbonated at 1000 °C for 1 hour and melted in a platinum-rhodium crucible in air at 1650 °C for 2 hours. The recovered glass had the chemical composition of $\text{Ca}_{0.98}\text{Si}_{1.01}\text{O}_3$ as given by electron microprobe analysis on six samples (Table S1). The mean bulk density of CaSiO_3 glass is 2.889 g/cm³ determined by Archimedes method. Sound velocities of CaSiO_3 glass were measured by ultrasonic technique and listed in Table S2. The CaSiO_3 glass was shaped into disks with a diameter of 20 mm and a thickness of 2 mm. Both faces of the sample disks were polished to parallel mirror surfaces within 1-2 μm uncertainty.

2.2 Shock wave experiments for Hugoniot

Shock wave experiments were performed using a two-stage light gas gun at Wuhan University of Technology. Schematic of experimental setup for Hugoniot equation of state of CaSiO_3 glass is shown in Figure S1(a). Two kinds of flyer and driver plates, Cu and Ta, were used in this study and their Hugoniot parameters are listed in Table S3 [*Mitchell and Nellis*, 1981]. The flyer velocities (W) were determined using the electro-magnetic method. The back plane of the sample disk was coated a film of copper with a thickness of about 100 nm to reflect the laser. Three optical fibers were mounted in a regular triangle on the front plane of sample disk and connect with a displacement interferometer system for any reflector (DISAR), which recorded optical fringe patterns and yielded the particle velocities of the driver/sample interface and free surface. If the sample keeps transparent under shock compression, the arrival times at the driver/sample interface (t_0) and free surface (t_1) can be obtained from particle velocity history of the

driver/sample interface and free surface (Figures S1(b) and S2). If the sample becomes opaque under shock compression, the t_0 and t_1 can be obtained from the optical fringe patterns recorded by DISAR (Figure S1(c)). The shock velocity (D) can be calculated according to the relationship of $D = \frac{H}{t_1 - t_0}$, where H is the sample's thickness. The elastic-plastic two-wave structure were observed in several experiments. The shock velocity of elastic wave was calculated by $D' = \frac{H}{t_1 - t_0}$, and the corresponding particle velocity (u') is obtained by the free surface approximation, $u' = \frac{u_{fs}}{2}$. The shock velocity of plastic wave was calculated by $D = \frac{H + u_{fs}(t_2 - t_1)}{t_2 - t_0}$, where u_{fs} , t_0 , t_1 , and t_2 were indicated in Figure S1(d). The particle velocity of the plastic wave is then calculated by impedance match between the driver plate and sample. The shock pressures and densities were calculated from the shock velocities and particle velocities with the Rankine-Hugoniot conservation equations [Forbes, 2012].

2.3 Shock wave experiments for sound velocity

The sound velocities of CaSiO_3 glass were determined by the optical analyser technique. Schematic of experimental setup for sound velocity of CaSiO_3 glass is shown in Figure S3(a). The flyer impact directly the sample CaSiO_3 glass without driver. Four optical fibers were mounted in a square on the front plane of sample disk to record optical fringe patterns and yield the particle velocity of the free surface. One optical fibers was mounted on the front plane of LiF window to obtain the particle velocity of sample/LiF interface. When impact, shock waves propagates in sample CaSiO_3 (D_s) and the flyer (D_f), respectively. Shock wave D_s arrives at the sample/LiF interface at t_0 . When shock wave D_f reaches the rear surface of the sample, it propagates forward as a rarefaction wave and reaches the sample/LiF interface at t_1 (Figures S3). The longitudinal

sound velocity of the sample (V_P^S) is calculated by $V_P^S = \frac{\rho_0^S}{\rho_s} \frac{d}{(t_1 - t_0) + d/D_s - h/D_f - h\rho_0^f / \rho_f V_P^f}$, where

ρ_0^S/ρ_0^f and ρ_s/ρ_f are the initial and compressed densities of sample/flyer, respectively; d and h are the thickness of the sample and flyer, respectively; V_P^f is the longitudinal sound velocity of the flyer. If the effect of reflected wave by the sample/LiF interface (point A) on the chasing rarefaction wave is ignorable due to the similar impedance of CaSiO₃ glass and LiF window (Figure S4), the bulk sound velocity of the sample (V_B^S) can be determined according to the elastic-plastic transition point at t_2 during unloading. Then the shear sound velocity (V_S) is calculated by

$$\text{means of } V_S = \sqrt{\frac{3}{4}(V_L^2 - V_B^2)}.$$

Table 1 The Hugoniot data of CaSiO₃ glass. W is the flyer velocity. u' and D' are the particle velocity and shock velocity of the elastic wave, respectively. ρ_{HEL} and P_{HEL} are density and shock pressure of Hugoniot elastic limit (HEL), respectively. u , D , ρ , and P are the particle velocity, shock velocity, density, and Hugoniot pressure of plastic wave, respectively.

No.	Flyer/ Driver	W (km/s)	u' (km/s)	D' (km/s)	ρ_{HEL} (g/cm ³)	P_{HEL} (GPa)	u (km/s)	D (km/s)	ρ (g/cm ³)	P (GPa)
1	Ta/Ta	3.736(19)	-	-	-	-	2.87(4)	7.72(9)	4.60(5)	64.1(12)
2	Ta/Ta	4.287(21)	-	-	-	-	3.26(5)	8.40(10)	4.72(6)	79.2(15)
3	Ta/Ta	3.258(16)	-	-	-	-	2.52(3)	7.21(8)	4.44(4)	52.5(9)
4	Ta/Ta	2.520(13)	0.48(1)	6.54(6)	3.12(1)	9.11(9)	1.98(1)	6.24(5)	4.22(2)	36.0(8)
5	Cu/Cu	2.336(12)	0.49(1)	6.53(6)	3.13(1)	9.10(8)	1.67(1)	5.89(4)	4.01(2)	29.1(5)
6	Cu/Cu	1.840(9)	0.53(1)	6.74(6)	3.14(1)	10.25(10)	1.302(8)	5.69(4)	3.69(1)	22.8(4)
7	Ta/Ta	2.753(14)	0.48(1)	6.83(7)	3.11(1)	9.51(9)	2.15(1)	6.59(6)	4.28(2)	41.2(10)

Table 2 Sound velocity of CaSiO₃ glass under shock compression.

No.	Flyer	W (km/s)	$u^\#$ (km/s)	D^* (km/s)	ρ (g/cm ³)	P (GPa)	V_P (km/s)	V_B (km/s)	V_S (km/s)
1	Ta	4.689(23)	3.51	8.82	4.79	89.3	11.01(30)	8.94(20)	5.57(51)
2	Ta	4.468(22)	3.35	8.57	4.75	83.0	10.36(28)	8.28(18)	5.40(45)

3	Ta	4.762(24)	3.57	8.93	4.81	92.2	11.29(33)	9.12(22)	5.77(55)
4	Ta	5.470(27)	4.13	9.86	4.97	117.6	13.24(50)	10.67(32)	6.79(82)
5	Ta	5.327(27)	4.00	9.66	4.94	111.7	12.61(45)	10.33(30)	6.27(77)

Particle velocity (u) is calculated according to impedance match.

* Shock velocity (D) is calculated from the linear D - u relation.

3 Results and discussions

3.1 Hugoniot of CaSiO_3 glass under shock compression

The Hugoniot data of CaSiO_3 glass are summarized in Table 1. The Hugoniot elastic limits (HEL) were calculated from elastic-plastic two-wave structure of four experiments (No. 4-7). The shock velocities (D) and corresponding particle velocities (u) are plotted in Figure 1, which can be divided into two linear regions. The D - u data were fitted to a linear relation of $D = C_0 + \lambda u$, where C_0 and λ are Hugoniot parameters. The linear fitting yield $D = 4.98 + 0.54u$ and $D = 2.95(11) + 1.67(5)u$ for two linear regions. The obtained C_0 (4.98 km/s) of the low shock velocity region is very close to the bulk sound velocity ($V_B = 5.117$ km/s) measured from ultrasonic measurements at ambient conditions. The cross point of two linear regions indicates the glass-crystalline phase transition of CaSiO_3 under shock compression. Previous shock wave data using wollastonite as the initial material are also plotted in Figure 1 for comparison [Marsh, 1980; Simakov and Trunin, 1980]. In spite of the same starting material, three sets of shock wave data of wollastonite are dispersive and inconsistent with each other, especially at low particle velocity range. At particle velocity above 2.2 km/s, the shock data of wollastonite display similar slope and trend to those of our study, indicating that both CaSiO_3 glass and wollastonite may transform into another crystalline phase.

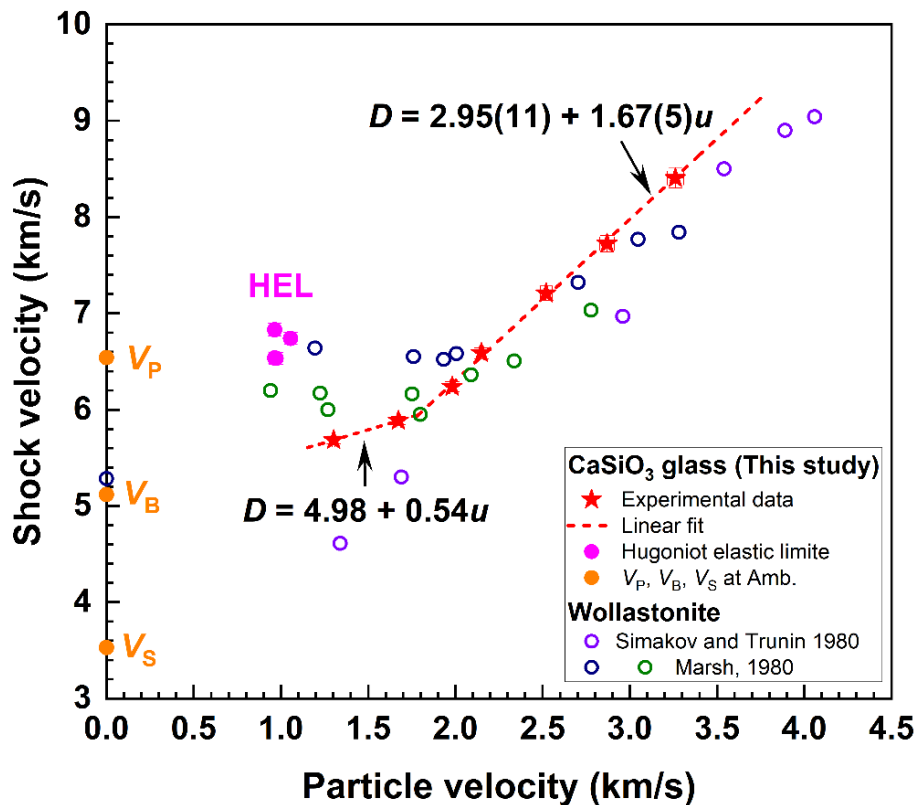


Figure 1 Shock velocity (D)-particle velocity (u) relation for CaSiO_3 glass. The dashed lines are linear fits to the Hugoniot data. V_P , V_B , and V_S are longitudinal, bulk, and transverse sound velocities of CaSiO_3 glass at ambient conditions, respectively. The Hugoniot elastic limit (HEL) of CaSiO_3 glass is shown in magenta circle. The open circles represent wollastonite under shock compression [Marsh, 1980; Simakov and Trunin, 1980].

The Hugoniot pressure (P) and density (ρ) of CaSiO_3 glass under shock compression are presented in Figure 2. The P - ρ curve of CaSiO_3 glass can be divided into three parts, a low pressure elastic region from Amb. to HEL, an intermediate region from HEL to about 34 GPa, and a high pressure region above 34 GPa. The HEL of CaSiO_3 glass ranges from 9.1 to 10.3 GPa. The abrupt change in compressibility along the Hugoniot at about 34 GPa is attributed to the glass-crystalline phase change of CaSiO_3 . Considering the pressure (P)-temperature (T) conditions of shock

compression, we preliminary inference that the CaSiO_3 glass transforms to the crystalline davemaoite above 34 GPa. A similar phenomenon has been reported on Hugoniot curve of amorphous SiO_2 [Marsh, 1980], which is plotted in Figure 2 for comparison. The Hugoniot curve of amorphous SiO_2 also consists of three regions. The abrupt change at 35 GPa is due to the transformation of a dense amorphous structure to polycrystalline stishovite, which is verified by plate-impact experiments and pulsed synchrotron X-ray diffraction [Tracy *et al.*, 2018].

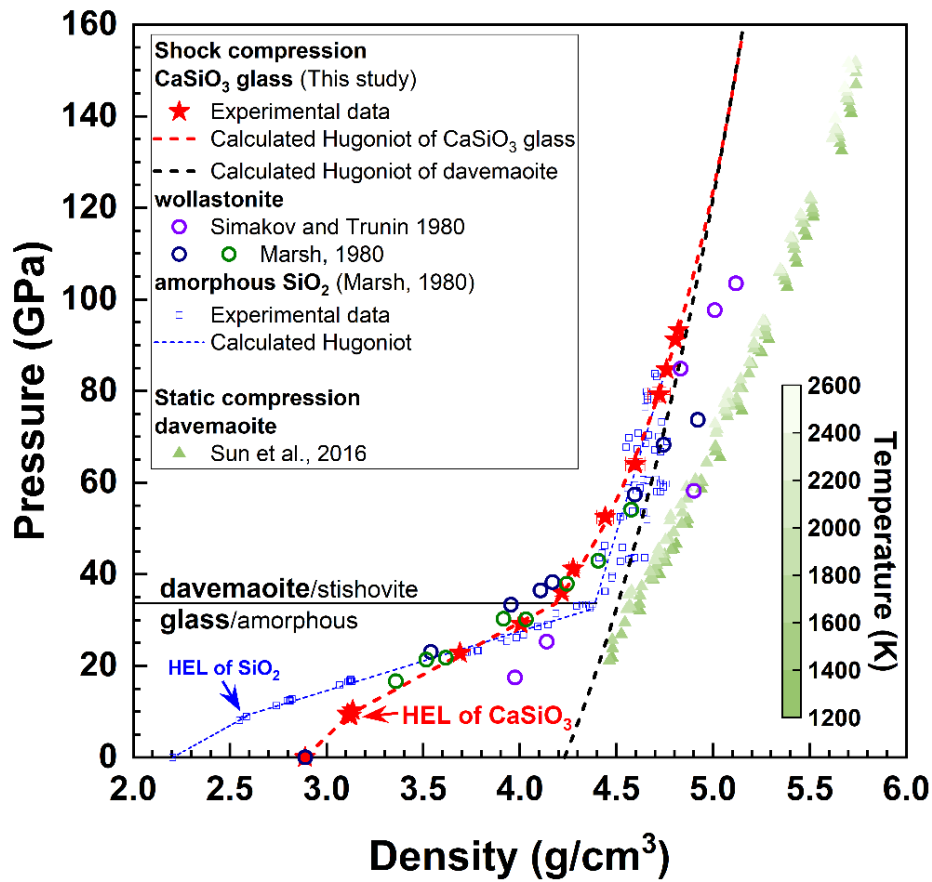


Figure 2 Hugoniot pressure (P) and density (ρ) of CaSiO_3 glass under shock compression. Red stars are experimental data. The red dashed line is the calculated Hugoniot curve of CaSiO_3 glass according to D - u linear relation. The black dashed line is the calculated Hugoniot equation of state for davemaoite by the Mie-Grüneisen equation of state. The open circles represent wollastonite

under shock compression [Marsh, 1980; Simakov and Trunin, 1980]. The experimental data and calculated Hugoniot curve of amorphous SiO₂ are shown in blue for comparison [Marsh, 1980]. HEL indicates Hugoniot elastic limit. The static experimental data of davemaoite are plotted in green triangles with color map [Sun *et al.*, 2016].

The Hugoniot of CaSiO₃ glass is compared with previous shock wave data using wollastonite as starting material (Figure 2). Crystalline wollastonite has almost the same initial density (2.89 g/cm³) as CaSiO₃ glass. The Hugoniot P - ρ of wollastonite from Marsh (1980) shows similar trend as that of CaSiO₃ glass at density range less than 4.6 g/cm³, but there is a significant deviation at greater density range. Despite the same starting material, the P - ρ of wollastonite from Marsh [1980] is different with that of Simakov and Trunin [1980] at density lower than 4.4 g/cm³, but they have similar trend at greater density. The Hugoniot data of both CaSiO₃ glass and wollastonite deviate from the isothermals of davemaoite under static compression [Sun *et al.*, 2016]. It indicates that both CaSiO₃ glass and wollastonite under shock compression have very high shock temperature.

3.2 Thermal equation of state of davemaoite

A theoretical Hugoniot equation of state for davemaoite has been calculated using the Mie-Grüneisen equation of state:

$$\frac{1}{2}P_H(V_{00} - V) = E_S + \frac{V}{\gamma}(P_H - P_S) + E_{tr}. \quad (1)$$

Here V is the Hugoniot specific volume; V_0 and V_{00} are the ambient specific volume of davemaoite and CaSiO₃ glass, respectively; γ is the Grüneisen parameter of davemaoite; P_S and P_H are the isentrope and Hugoniot pressure, respectively; E_S is the isentrope energy and E_{tr} is the energy of

phase transition from CaSiO₃ glass to davemaoite. Rearrangement of Eq. 1 gives the Hugoniot pressure:

$$P_H = \frac{P_S - \frac{\gamma}{V}(E_S + E_{tr})}{1 - \frac{\gamma(V_{00} - V)}{2V}}. \quad (2)$$

The Grüneisen parameter is assumed to depend only on volume:

$$\gamma = \gamma_0 \left(\frac{V}{V_0}\right)^q. \quad (3)$$

The isentrope pressure is determined by an isentropic Birch-Murnaghan equation of state:

$$P_S = \frac{3}{2}K_{0S} \left[\left(\frac{V_0}{V}\right)^{7/3} - \left(\frac{V_0}{V}\right)^{5/3} \right] \left[1 + \frac{3}{4}(K'_{0S} - 4) \left(\left(\frac{V_0}{V}\right)^{2/3} - 1 \right) \right], \quad (4)$$

where K_{0S} and K'_{0S} are the isentropic bulk modulus and its pressure derivative, respectively. The isentrope energy is calculated from numerical integration of the isentropic compression curve:

$$E_S = - \int_{V_0}^V P_S dV. \quad (5)$$

The thermodynamic parameters in Mie-Grüneisen equation of state are listed in Table 3. The calculated Hugoniot equation of state for davemaoite are plotted in Figure 2. The Hugoniot curve of CaSiO₃ glass is well consistent with that of davemaoite above 120 GPa, but they are far from each other below 120 GPa to 34 GPa. The pressure region of 34-120 GPa is a mixed region of davemaoite and the low pressure phases, and the measured density by shock wave experiments in the mixed phase region likely represents that of the mixture between davemaoite and low pressure phases. The minimum shock pressure required to completely transform CaSiO₃ glass into davemaoite is about 120 GPa, which is much higher than the stable P-T conditions of davemaoite in static experiments. It is reasonable to observe this phenomenon on shocked CaSiO₃ glass, similar to MgSiO₃ under shock compression with various low pressure starting materials. The bridgmanite stable zone in shock experiments is above 90 GPa [Deng *et al.*, 2008], which is also much higher than the stable P-T conditions of bridgmanite in static compression experiments.

Table 3 The thermodynamic parameters in Mie-Grüneisen equation of state

Parameter	ρ_{00} (g/cm ³)	ρ_0 (g/cm ³)	K_{0S} (GPa)	K_{0S}'	E_{tr}	γ_0	q
Value	2.889	4.232	248	4.2	0	1.9	1.1
Reference	This study	Gréaux 2019	Gréaux 2019	Gréaux 2019	-	This study	This study

3.3 P-T phase diagram of davemaoite

The Hugoniot temperature of davemaoite has been calculated by numerical integration of the heat capacity (C_V):

$$\int_{T_S}^{T_H} C_V dT = \int_{P_S}^{P_H} \frac{V}{\gamma} dP. \quad (6)$$

C_V can be represented by the Dulong-Petit limit with $C_V = 3R/\mu$, where R is the ideal gas constant and μ is the molar mass. The isentrope temperature (T_S) is:

$$T_S = T_0 \exp\left(\int_V^{V_0} \frac{\gamma}{V} dV\right). \quad (7)$$

Combing Eqs. (6) and (7), the Hugoniot temperature of davemaoite is:

$$T_H = T_S + \frac{V}{\gamma} \frac{P_H - P_S}{C_V}. \quad (8)$$

The calculated Hugoniot temperature of davemaoite has been plotted in Figure 3. Davemaoite upon shock compression has very high Hugoniot temperature. The Hugoniot temperature would reach the melting temperature at about 115 GPa, compared with the melting curve predicted by *Yin et al.* [2023] that gives the highest melting temperature of davemaoite to date. The phase boundaries of solid phases of CaSiO_3 have also been plotted in Figure 3 for discussion. CaSiO_3 is stable in wollastonite structure at ambient conditions, which transforms into breyite above 4 GPa [Essene, 1974]. Breyite decomposes into an assemblage of larnite (Ca_2SiO_4) and titanite (CaSi_2O_5) above 8 GPa [Gasparik et al., 1994]. Larnite and titanite react and form the perovskite phase above 13 GPa [Sueda et al., 2006], where the tetragonal perovskite is stable below 500 K while the

davemaoite with a cubic perovskite structure is stable above 500 K [Komabayashi *et al.*, 2007]. Considering the P-T conditions of shock compression and based on the P-T phase diagram of CaSiO_3 , we identify the CaSiO_3 glass transforms to a crystalline mixture of davemaoite and low pressure phases above 34 GPa, and low pressure crystalline phases completely transform into davemaoite above 120 GPa (Figure 2).

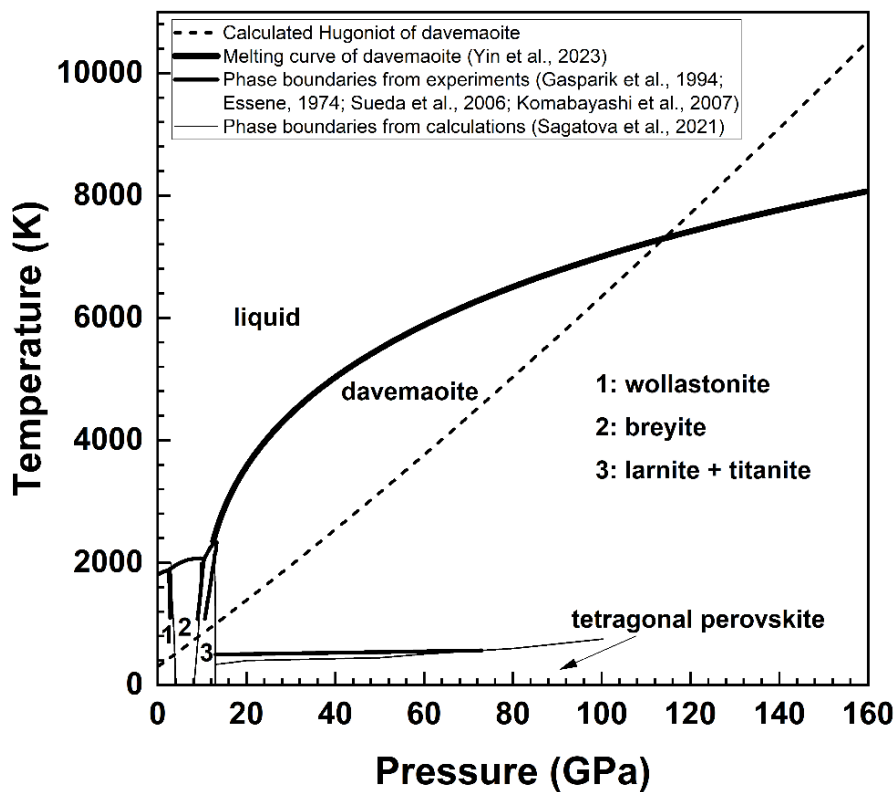


Figure 3 The calculated Hugoniot temperature of davemaoite is shown in dashed line. The thick solid line is the predicted melting curve of davemaoite [Yin *et al.*, 2023]. Phase boundaries of solid phases of CaSiO_3 from experiments and calculations are plotted in bold and thin solid lines, respectively [Essene, 1974; Gasparik *et al.*, 1994; Komabayashi *et al.*, 2007; Sagatova *et al.*, 2021; Sueda *et al.*, 2006].

3.4 Sound velocity of CaSiO₃ glass under shock compression

Five shock wave experiments for sound velocity of CaSiO₃ glass have been performed with the highest shock pressure of 117.6 GPa (Figures S5 and 4). According to the Hugoniot of CaSiO₃ glass discussed above, the pressure region of 34-120 GPa is a mixed region of davemaoite and the low pressure phases, thus the measured sound velocity of CaSiO₃ glass below 120 GPa represent that of the mixture between davemaoite and low pressure phases. Even so, the sound velocities of CaSiO₃ glass along Hugoniot provide some significant information.

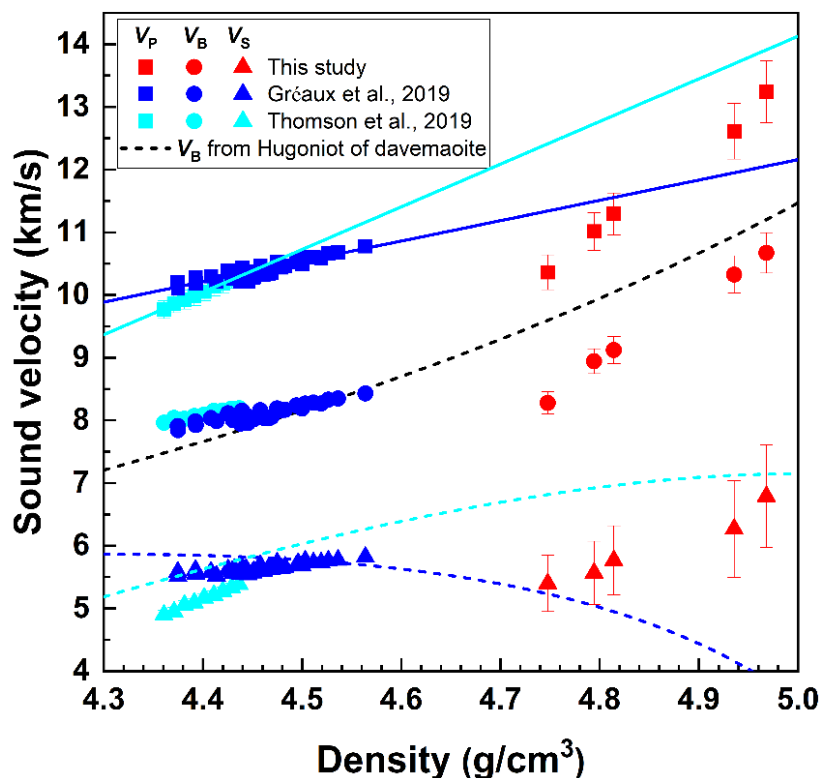


Figure 4 Sound velocities (V_P , V_B and V_S) and density of CaSiO₃ glass under shock compression. Sound velocities (V_P , V_B and V_S) of davemaoite from static compression experiments are shown in blue and cyan symbols [Gréaux et al., 2019; Thomson et al., 2019]. The blue and cyan solid lines represent the linear fits of V_P about density. V_B from Hugoniot of davemaoite are shown in black

dashed line. The blue and cyan dashed lines are the calculated V_S of davemaoite along Hugoniot from the linear extrapolation of V_P and Hugoniot V_B of davemaoite.

Sound velocities of davemaoite from static compression experiments have also been plotted for discussion. The one from *Gréaux et al.* [2019] ranges from 700 K and 12 GPa to 1700 K and 23 GPa. The other one from *Thomson et al.* [2019] is measured at 12 GPa and 473-1273 K. Suppose Birch's law, the linear density-sound velocity relationship, holds for the V_P of davemaoite. The two sets of static experimental data plotted in Figure 4 are not consistent with each other, indicating some unknown effect or systematic error due to measurement technique. The measured V_P along Hugoniot of CaSiO_3 glass below 100 GPa is much lower than linear extrapolations of V_P of davemaoite from static compression experiments due to the mixture of davemaoite and lower pressure phases. With increasing Hugoniot pressure above 110 GPa, the measured V_P along Hugoniot of CaSiO_3 glass approaches the linear extrapolation of *Thomson et al.* [2019] but drifts away from that of *Gréaux et al.* [2019]. The measured V_P at the highest Hugoniot pressure of 117.6 GPa in this study should be very close to the V_P of pure davemaoite.

The V_S at high pressure is typically affected by high temperature because of shear softening at high temperature, thus it is difficult to discuss the relationship of V_S and density at various pressures and temperatures. In addition, the calculated V_B from V_P and V_S is also temperature dependent at a constant density. Even so, the measured V_B along the Hugoniot of CaSiO_3 glass can be compared with the calculated V_B from Hugoniot of davemaoite. The measured V_B along the Hugoniot of CaSiO_3 glass is lower than the calculated V_B from Hugoniot of davemaoite, verifying that the shocked CaSiO_3 glass below 120 GPa is not a pure davemaoite. With the Hugoniot pressure increases, the measured V_B along the Hugoniot of CaSiO_3 glass gradually approaches the

calculated V_B from Hugoniot of davemaoite. Additionally, the V_S of davemaoite along Hugoniot are calculated from the linear extrapolations of V_P and Hugoniot V_B of davemaoite and are plotted in Figure 4. The derived V_S along Hugoniot of CaSiO_3 glass is higher than the calculated V_S of davemaoite from V_P of *Gréaux et al.* [2019] but gradually approaches that from V_P of *Thomson et al.* [2019] with increasing shock pressure.

It's worth noting that no melting is observed at Hugoniot pressure up to 117.6 GPa. The measured V_P along the Hugoniot of CaSiO_3 glass gradually increase with increasing shock pressure and do not present a pronounced decrease close to V_B even at 117.6 GPa, which is thought to be a sign of melting behavior, losing of shear stiffness. As discussed above in Figure 3, the calculated Hugoniot temperature of davemaoite would reach the melting temperature at about 115 GPa, in comparison with the predicted highest melting curve of davemaoite to date [*Yin et al.*, 2023]. Our measured V_P of CaSiO_3 up to 117.6 GPa provides a direct evidence that the melting temperature of davemaoite should be higher than those reported by now. Further sound velocity measurements above 120 GPa representing pure davemaoite are required in the future to discuss the relationship of sound velocity and density/pressure and confirm the melting behavior of davemaoite.

Acknowledgments

Authors acknowledge the financial supports from the National Natural Science Foundation of China (42274123 and 12105209) and the United Laboratory of High-Pressure Physics and Earthquake Science.

Reference

- Deng, L., Z. Gong, and Y. Fei (2008), Direct shock wave loading of MgSiO_3 perovskite to lower mantle conditions and its equation of state, *Phys. Earth Planet. Inter.*, 170(3-4), 210-214.
- Essene, E. (1974), High-pressure transformations in CaSiO_3 , *Contrib. Mineral. Petrol.*, 45(3), 247-250.

- Fei, Y., and S. J. Tracy (2024), High pressure and temperature experiments.
- Forbes, J. W. (2012), *Shock wave compression of condensed matter: a primer*, Springer.
- Fukao, Y., and M. Obayashi (2013), Subducted slabs stagnant above, penetrating through, and trapped below the 660 km discontinuity, *J. Geophys. Res. Solid Earth*, *118*(11), 5920-5938.
- Garnero, E. J., A. K. McNamara, and S. H. Shim (2016), Continent-sized anomalous zones with low seismic velocity at the base of Earth's mantle, *Nat. Geosci.*, *9*(7), 481-489.
- Gasparik, Tibor, Wolf, and Kenneth (1994), Experimental determination of phase relations in the CaSiO₃ system from 8 to 15 GPa, *Am. Mineral.*
- Gréaux, S., T. Irifune, Y. Higo, Y. Tange, T. Arimoto, Z. Liu, and A. Yamada (2019), Sound velocity of CaSiO₃ perovskite suggests the presence of basaltic crust in the Earth's lower mantle, *Nature*, *565*, 218-222.
- Hofmann, A. W. (1988), Chemical differentiation of the Earth: the relationship between mantle, continental crust, and oceanic crust, *Earth Planet. Sci. Lett.*, *90*(3), 297-314.
- Immoor, J., L. Miyagi, H.-P. Liermann, S. Speziale, K. Schulze, J. Buchen, A. Kurnosov, and H. Marquardt (2022), Weak cubic CaSiO₃ perovskite in the Earth's mantle, *Nature*, *603*(7900), 276-279.
- Irifune, T. (1994), Absence of an aluminous phase in the upper part of the Earth's lower mantle, *Nature*, *370*, 131-133.
- Irifune, T., T. Shinmei, C. A. McCammon, N. Miyajima, D. C. Rubie, and D. J. Frost (2010), Iron partitioning and density changes of pyrolyte in Earth's lower mantle, *Science*, *327*(5962), 193-195.
- Kaminski, E., and M. Javoy (2013), A two-stage scenario for the formation of the Earth's mantle and core, *Earth Planet. Sci. Lett.*, *365*, 97-107.
- Karki, B. B., and J. Crain (1998), First-principles determination of elastic properties of CaSiO₃ perovskite at lower mantle pressures, *Geophys. Res. Lett.*, *25*(14).
- Kawai, K., and T. Tsuchiya (2014), P-V-T equation of state of cubic CaSiO₃ perovskite from first-principles computation, *J. Geophys. Res. Solid Earth*, *119*(4), 2801-2809.
- Kawai, K., and T. Tsuchiya (2015), Small shear modulus of cubic CaSiO₃ perovskite, *Geophys. Res. Lett.*, *42*(8), 2718-2726.
- Komabayashi, T., K. Hirose, N. Sata, Y. Ohishi, and L. S. Dubrovinsky (2007), Phase transition in CaSiO₃ perovskite, *Earth Planet. Sci. Lett.*, *260*(3), 564-569.
- Lee, C.-T. A., P. Luffi, T. Höink, J. Li, R. Dasgupta, and J. Hernlund (2010), Upside-down differentiation and generation of a 'primordial' lower mantle, *Nature*, *463*(7283), 930-933.
- Li, L., D. J. Weidner, J. Brodholt, D. Alfe, G. David Price, R. Caracas, and R. Wentzcovitch (2006), Elasticity of CaSiO₃ perovskite at high pressure and high temperature, *Phys. Earth Planet. Inter.*, *155*(3), 249-259.
- Liu, L. G., and A. Ringwood, E. (1975), Synthesis of a perovskite-type polymorph of CaSiO₃, *Earth Planet. Sci. Lett.*, *28*(2), 209-211.
- Mao, H.-K., B. Chen, J. Chen, K. Li, J.-F. Lin, W. Yang, and H. Zheng (2016), Recent advances in high-pressure science and technology, *Matter and Radiation at Extremes*, *1*(1), 59-75.
- Marsh, S. P. (1980), *LASL Shock Hugoniot Data*, Univ. California Press, Berkeley.
- Mitchell, A., and W. Nellis (1981), Shock compression of aluminum, copper, and tantalum, *J. Appl. Phys.*, *52*(5), 3363-3374.
- Murakami, M., A. Khan, P. A. Sossi, M. D. Ballmer, and P. Saha (2024), The Composition of Earth's Lower Mantle, *Annu. Rev. Earth Planet. Sci.*, *52*(1), 605-638.
- Noguchi, M., T. Komabayashi, K. Hirose, and Y. Ohishi (2013), High-temperature compression experiments of CaSiO₃ perovskite to lowermost mantle conditions and its thermal equation of state, *Phys. Chem. Miner.*, *40*(1), 81-91.
- Price, G. D. (2010), *Treatise on Geophysics, Volume 2: Mineral Physics*.
- Ricolleau, A., J. P. Perrillat, G. Fiquet, I. Daniel, J. Matas, A. Addad, N. Menguy, H. Cardon, M. Mezouar, and N. Guignot (2010), Phase relations and equation of state of a natural MORB: Implications for the density profile of subducted oceanic crust in the Earth's lower mantle, *J. Geophys. Res.*, *115*(B8), B08202.
- Sagatova, D., A. Shatskiy, N. Sagatov, and K. Litasov (2021), Phase relations in CaSiO₃ system up to 100 GPa and 2500 K, *Geochemistry International*, *59*(8), 791-800.
- Shen, G., and Y. Wang (2014), High-pressure apparatus integrated with synchrotron radiation, *Rev. Mineral. Geochem.*, *78*(1), 745-777.
- Shen, G., and H. K. Mao (2016), High-pressure studies with x-rays using diamond anvil cells, *Reports on progress in Physics*, *80*(1), 016101.
- Shim, S. H., T. S. Duffy, and G. Shen (2000), The stability and P-V-T equation of state of CaSiO₃ perovskite in the Earth's lower mantle, *J. Geophys. Res. Solid Earth*, *105*(B11), 25955-25968.
- Simakov, G. V., and R. F. Trunin (1980), Minerals compression by shock waves, *Izv. Akad. Nauk SSSR. Fiz. Zemli*, *2*,

77-81.

Stixrude, L., C. Lithgow-Bertelloni, B. Kiefer, and P. Fumagalli (2007), Phase stability and shear softening in CaSiO_3 perovskite at high pressure, *Phys. Rev. B*, 75(2), 024108.

Sueda, Y., T. Irifune, A. Yamada, T. Inoue, X. Liu, and K. i. Funakoshi (2006), The phase boundary between CaSiO_3 perovskite and $\text{Ca}_2\text{SiO}_4 + \text{CaSi}_2\text{O}_5$ determined by in situ X-ray observations, *Geophys. Res. Lett.*, 33(10).

Sun, N., Z. Mao, S. Yan, X. Wu, V. Prakapenka, and J.-F. Lin (2016), Confirming a pyrolitic lower mantle using self-consistent pressure scales and new constraints on CaSiO_3 perovskite, *J. Geophys. Res. Solid Earth*, 121(7), 4876-4894.

Thomson, A. R., W. A. Crichton, J. P. Brodholt, I. G. Wood, N. C. Siersch, J. M. R. Muir, D. P. Dobson, and S. A. Hunt (2019), Seismic velocities of CaSiO_3 perovskite can explain LLSVPs in Earth's lower mantle, *Nature*, 572(7771), 643-647.

Tracy, S. J., S. J. Turneure, and T. S. Duffy (2018), In situ x-ray diffraction of shock-compressed fused silica, *Phys. Rev. Lett.*, 120(13), 135702.

Tschauner, O., C. Ma, J. R. Beckett, C. Prescher, V. B. Prakapenka, and G. R. Rossman (2014), Discovery of bridgmanite, the most abundant mineral in Earth, in a shocked meteorite, *Science*, 346(6213), 1100-1102.

Tschauner, O., S. Huang, S. Yang, M. Humayun, W. Liu, S. N. Gilbert Corder, H. A. Bechtel, J. Tischler, and G. R. Rossman (2021), Discovery of davemaoite, CaSiO_3 -perovskite, as a mineral from the lower mantle, *Science*, 374(6569), 891-894.

Wang, Y., D. J. Weidner, and F. Guyot (1996), Thermal equation of state of CaSiO_3 perovskite, *J. Geophys. Res. Solid Earth*, 101(B1), 661-672.

Waszek, L., N. C. Schmerr, and M. D. Ballmer (2018), Global observations of reflectors in the mid-mantle with implications for mantle structure and dynamics, *Nat. Commun.*, 9(1), 385.

Wentzcovitch, R. M., and L. Stixrude (2018), *Theoretical and computational methods in mineral physics: Geophysical applications*, Walter de Gruyter GmbH & Co KG.

Wu, F., Y. Sun, T. Wan, S. Wu, and R. M. Wentzcovitch (2024), Deep-Learning-Based Prediction of the Tetragonal \rightarrow Cubic Transition in Davemaoite, *Geophys. Res. Lett.*, 51(12), e2023GL108012.

Yin, K., A. B. Belonoshko, Y. Li, and X. Lu (2023), Davemaoite as the mantle mineral with the highest melting temperature, *Science Advances*, 9(49), eadj2660.

Zhang, Y., D. Zhao, M. Matsui, and G. Guo (2006), Equations of state of CaSiO_3 Perovskite: a molecular dynamics study, *Phys. Chem. Miner.*, 33(2), 126-137.

arXiv

Supporting Information for

Hugoniot equation of state and sound velocity of CaSiO₃ glass under shock compression

Ye Wu ¹, Qing Zhang ¹, Yishi Wang ¹, Yu Hu ¹, Zehui Li ¹, Zining Li ¹, Chang Gao ¹, Xun Liu ¹,
Haijun Huang ¹, Yingwei Fei ²

¹ School of Physics and Mechanics, Wuhan University of Technology, Wuhan, Hubei 430070, China

² Earth and Planets Laboratory, Carnegie Institution for Science, Washington, DC 20015, USA

Corresponding author: Xun Liu (xun_liu@whut.edu.cn) and Yingwei Fei (yfei@carnegiescience.edu)

Contents of this file

Tables S1 to S3

Figures S1 to S2

Table S1 Electron microprobe analysis of CaSiO₃ glass

Oxide	sample 1	sample 2	sample 3	sample 4	sample 5	sample 6	Cation	Apfu*
CaO (wt %)	47.686	47.625	47.534	47.592	47.279	47.702	Ca ²⁺	0.98
SiO ₂ (wt %)	52.348	52.613	52.088	52.542	52.319	52.537	Si ⁴⁺	1.01
Total (wt %)	100.033	100.238	99.622	100.134	99.598	100.239	-	-

Apfu*: Atoms per formula unit, normalized to three oxygen atoms.

Table S2 Density and sound velocities of CaSiO₃ glass at ambient conditions

Density	2.889 g/cm ³
Longitudinal sound velocity	6.542 km/s
Transverse sound velocity	3.530 km/s
Buck sound velocity	5.117 km/s

Table S3 Hugoniot parameters of flyer and driver plates

Material	ρ_0 (g/cm ³)	C_0 (km/s)	λ
Cu	8.935	3.933	1.500
Ta	16.654	3.293	1.307

ρ_0 is density of Cu or Ta at ambient conditions. C_0 and λ are parameters of shock velocity-particle velocity relationship of Cu or Ta.

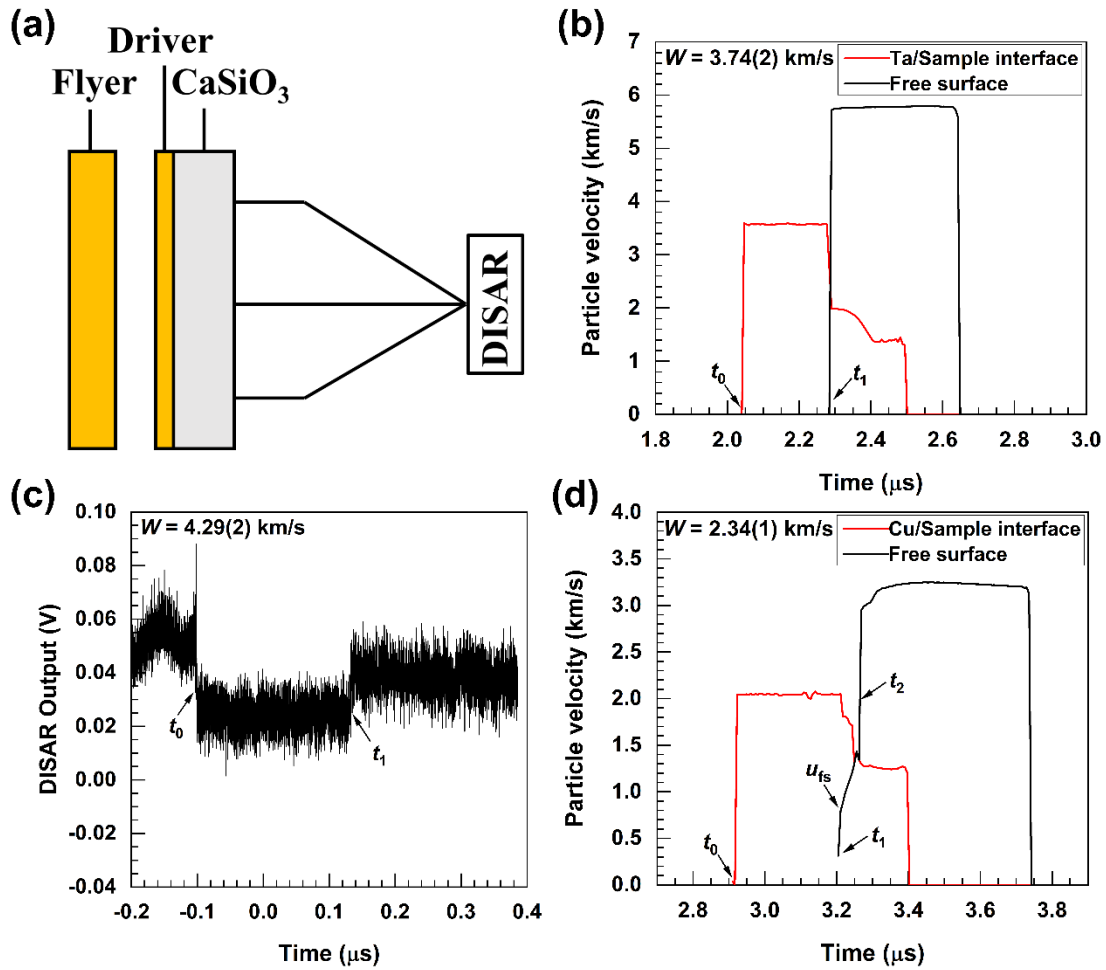


Figure S1 (a) Schematic of experimental setup for Hugoniot equation of state of CaSiO_3 glass under shock compression. (b) and (d) The particle velocity history of the driver/sample interface and free surface for experiments No. 1 and No. 5, respectively. (c) The optical fringe patterns recorded by DISAR for experiment No. 2.

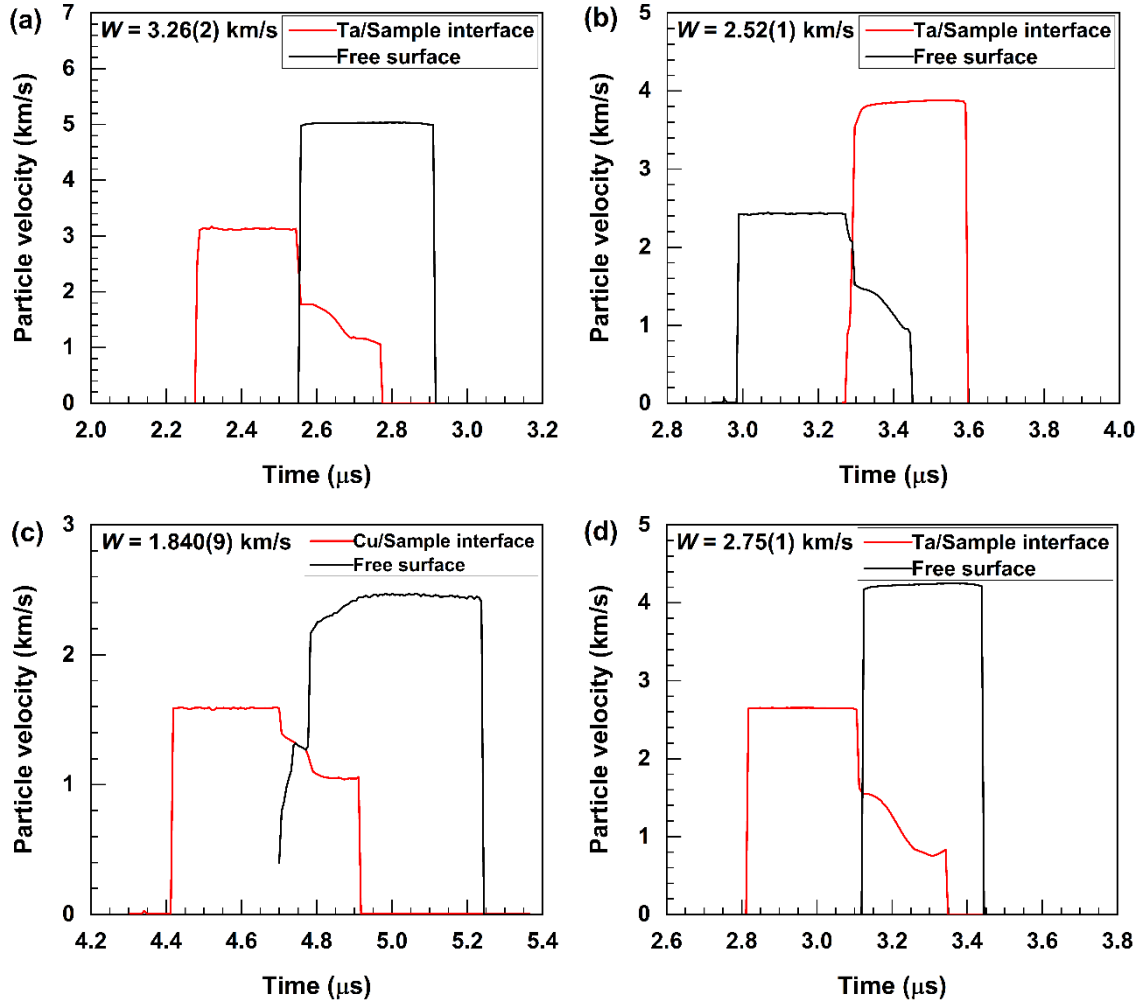


Figure S2 The particle velocity history of the driver/sample interface and free surface for experiments No. 3 (a), No. 4 (b), No. 6 (c) and No. 7 (d), respectively.

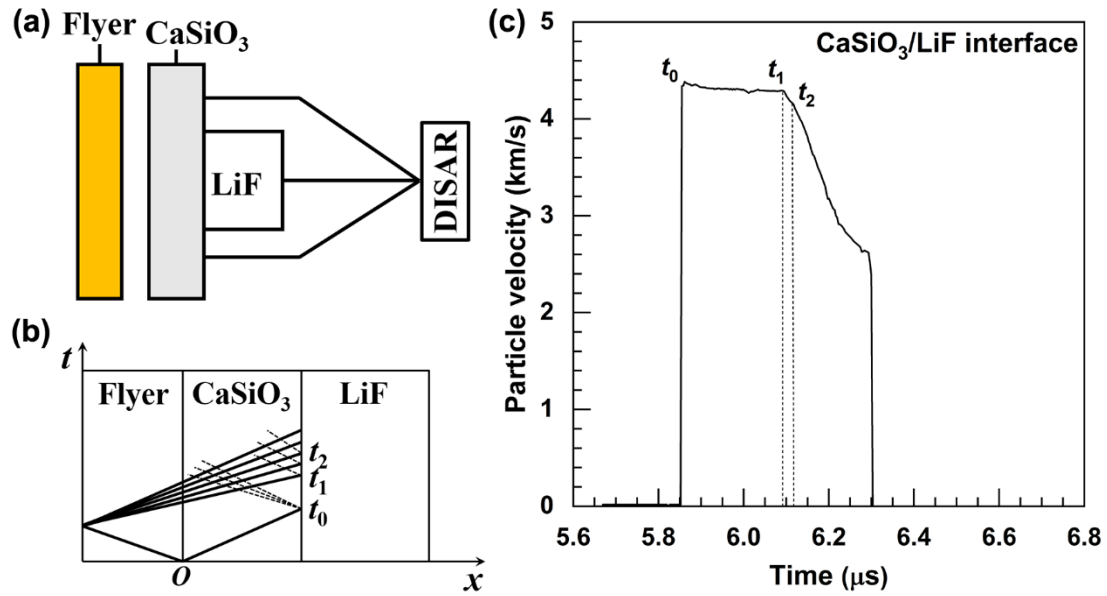


Figure S3 (a) Schematic of experimental setup for sound velocity of CaSiO₃ glass under shock compression. (b) Schematic distance-time diagram of shock wave propagation after impact. (c) The particle velocity of the CaSiO₃/LiF interface.

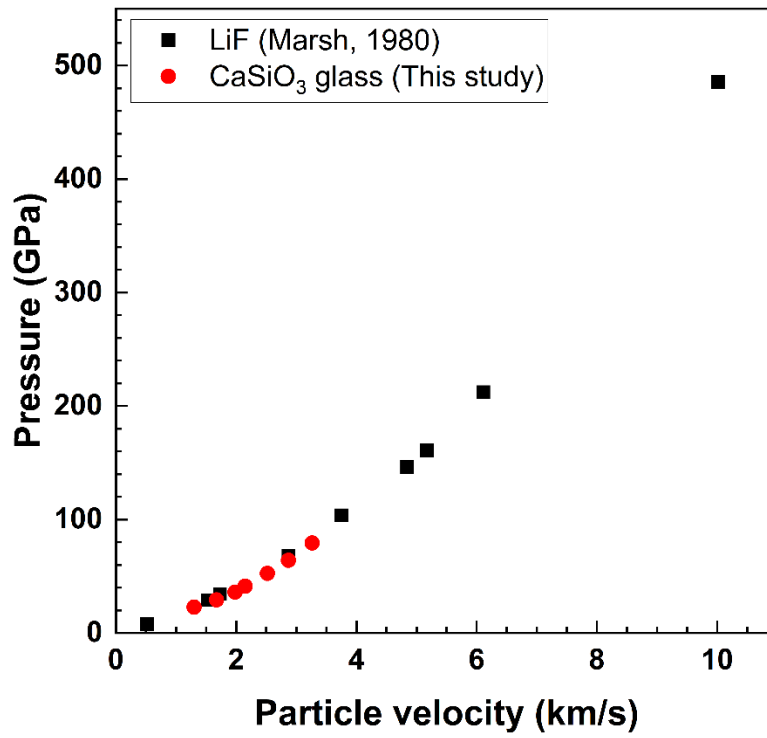


Figure S4 The pressure and particle velocity of CaSiO₃ glass and LiF under shock compression [Marshall, 1980].

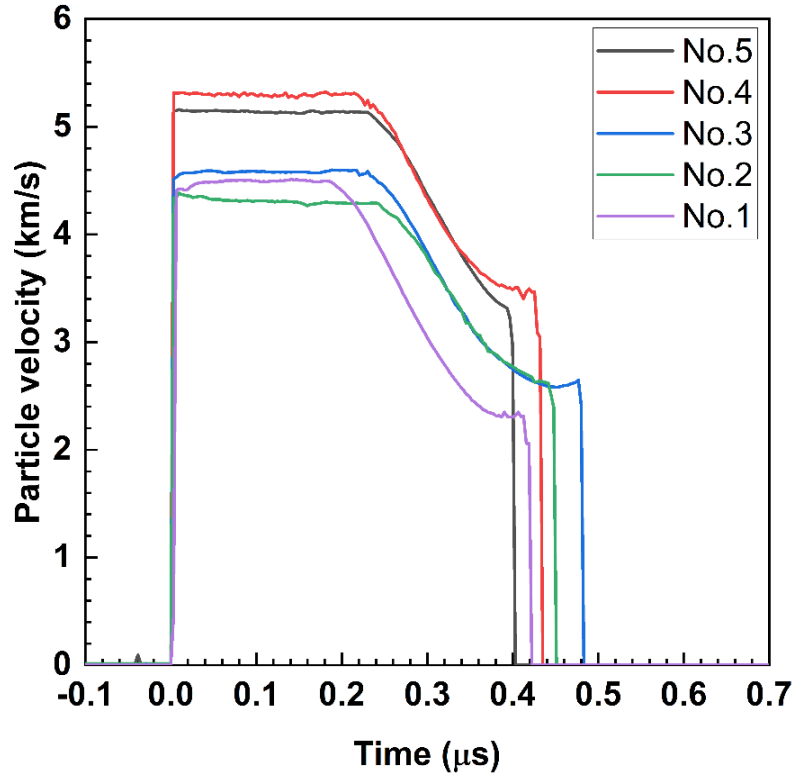


Figure S5 The particle velocity of the CaSiO₃/LiF interface for five measurements of sound velocity of CaSiO₃ glass under shock compression. The time of shock wave arriving at the sample/LiF interface (t_0) for five experiments has been moved to zero for comparison.